Geologic and Geodetic Aspects of the December 2004 Great Sumatra-Andaman and 2005 Nias-Simeulue Earthquakes

Kenneth W. Hudnut[a)]

Geologic data from field observations and satellite imagery analysis contribute a constraint on the "pivot line" between uplift and subsidence of coral reefs, indicating the downdip rupture extent. Geodetic global positioning system (GPS) data contribute vector displacements of points on islands along the archipelago, indicating amount and direction of slip alongstrike of the rupture. Geodetic and geologic data are sensitive not only to rapid coseismic fault movement, but also to slower motion across the plate interface that occurs postseismically. Consequently, the source dimensions and slip pattern estimates based on various geodetic and geologic data differ from purely seismic estimates. A more complete understanding is emerging, based upon joint inversions that use various combinations of all available data, of ways in which sudden slip and gradual afterslip occurred in each of these two major plate boundary ruptures. [DOI: 10.1193/1.2222383]

INTRODUCTION

The northern two-thirds of the Sunda megathrust that broke in the 26 December 2004 Sumatra-Andaman event (M=9.2) had not been considered seismogenic (McCann et al. 1979), much less capable of generating a basinwide tsunami (Figure 1). McCann et al. accurately stated, "The portion of the Sunda arc along the Andaman and Nicobar Islands is characterized by oblique convergence. There are no great earthquakes or extensive tsunamis reported historically." After analyzing studies describing the documented historical earthquakes and tsunamis from about 6° N to 16° N in further detail (Figure 1), McCann et al. then surmised, "Hence, there may not appear to be great earthquakes associated with the Sunda arc in the Andaman-Nicobar region." This became the rational basis for generally accepted understanding, but then unfortunately, almost as if to prove that scientists had been terribly wrong, the earthquake and tsunami of 26 December 2004 occurred.

Taking into account all prior data, regional seismic hazard forecasts (e.g., Giardini et al. 2003, Petersen et al. 2004) had not fully anticipated this great tsunamigenic earthquake because of the highly oblique plate convergence angle. Stress caused by this event evidently led to the large 28 March 2005 Nias-Simeulue event (M=8.6) directly to the south (McCloskey et al. 2005), which then led to concerns of a continuing domino effect

[a)] U.S. Geological Survey, 525 South Wilson Ave., Pasadena, CA 91106

Earthquake Spectra, Volume 22, No. S3, pages S13–S42, June 2006; © 2006, Earthquake Engineering Research Institute

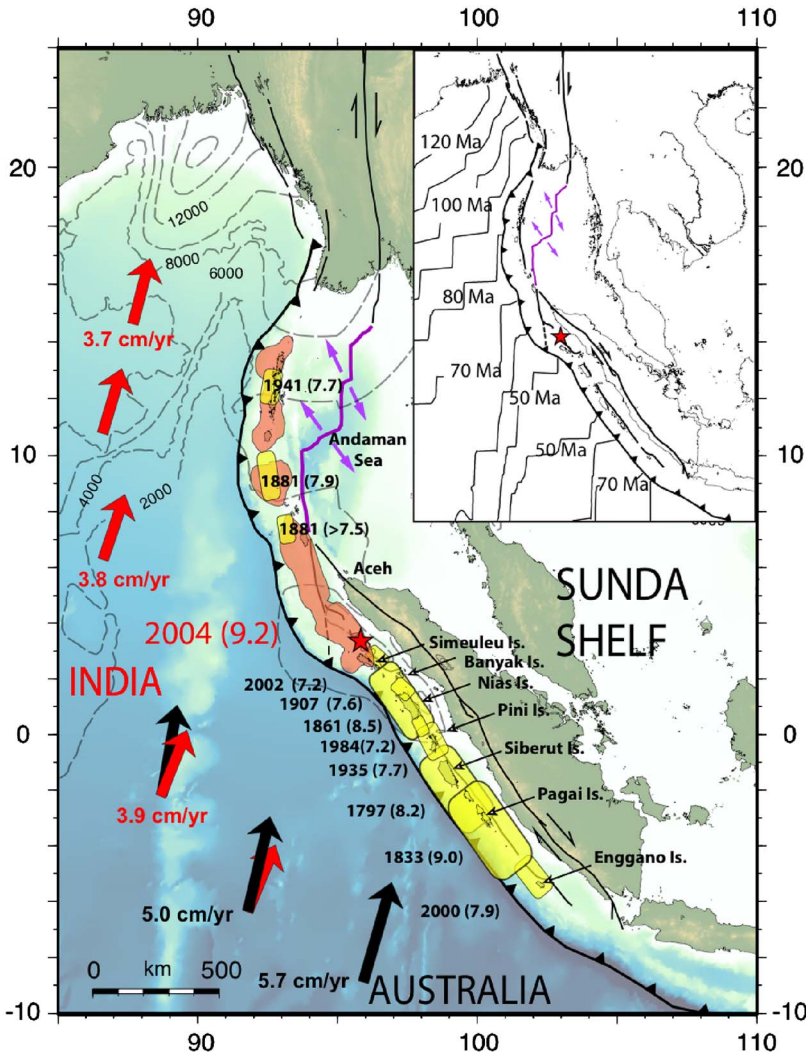

Figure 1. The Sunda megathrust plate boundary, along which the 2004 Sumatra-Andaman and 2005 Nias-Simeulue earthquakes occurred. Plate motion vectors relative to Sunda (black arrows for Australia, red [in grayscale: gray] for India) and plate ages and major boundaries are shown (inset). Rupture zones of historic and prehistoric earthquakes are shown in yellow (in grayscale: light gray), and areas of >5 m slip in the 2004 earthquake are shown in orange (in grayscale: darker gray). Sediment thickness contours at 2,000-m intervals are shown as dashed lines (from Subarya et al. 2006).

toward the southeast along the megathrust (Nalbant et al. 2005). Between 1° S and 5° S, the megathrust had last ruptured in a major event pair that occurred in 1797 and 1833 (McCann et al. 1979; Newcomb and McCann 1987; Zachariasen et al. 1999; Natawid-

jaja et al. 2004, 2006). This recently unruptured segment therefore remains a source of heightened concern, creating great uncertainty for the western Sumatra coastal cities of Padang and Bengkulu (Sieh 2005).

Slip during the Sumatra-Andaman and Nias-Simeulue events was heterogeneous in both space and time, and it achieved a wide range of slip amounts and slip velocities across very large areas of the plate interface. The most rapid portions of the slip events radiated seismic energy, as summarized by Kanamori (2006, this issue). The relatively rapid slip also produced permanent displacement of the islands and seafloor along the plate boundary. The dynamic oscillatory motions and also the rapidly occurring motions that produce static displacements of the solid earth both couple energy into the ocean, generating a tsunami. The damaging effects of the shaking and tsunami, however, were certainly primarily produced by the relatively rapid rupture propagation along the plate interface.

Also important, however, were the continuing slow movements along the plate boundary interface after both events, typically called *postseismic creep* or *afterslip* (Scholz 1989, 2002). These motions produced ongoing large static displacements across the region (e.g., Vigny et al. 2005, Subarya et al. 2006). For the Sumatra-Andaman event, both rapid and slower slip were sufficiently large to be geodetically recorded locally, regionally, and worldwide (e.g., Banerjee et al. 2005, Vigny et al. 2005, Kreemer et al. 2006). To understand geodynamics, plate boundary processes, and long-term hazards, we need a comprehensive understanding of not only the rapid coseismic slip, but also the slow aseismic fault slip following these earthquakes. It is recognized that the afterslip contribution to an event's total moment can be large (e.g., Heki 1997) and can obscure the pattern of immediate coseismic slip (e.g., Ji et al. 2003). In the case of the Sumatra-Andaman event, afterslip contributions during the first month were as much as 30% of the coseismic slip (e.g., Subarya et al. 2006, Chlieh et al. 2006), whereas nine months after the Nias-Simeulue event, the afterslip reached up to 25% of the coseismic slip (Hsu et al. 2006). Prolonged and aseismic transient behavior on the plate interface, while complicating interpretation of the seismological data, may eventually reveal previously unknown phenomena associated with such large megathrust events. Furthermore, the geodetic data can be alternatively explained entirely by asthenosphere relaxation (Pollitz et al. 2006a).

Sudden release of accumulated relative plate motion, in the form of slip across the Sunda megathrust plate interface, produced a variety of effects that have already been extensively observed and reported elsewhere. Initially, seismic data were used to construct source models of each of the two events (e.g., Ammon et al. 2005; Kanamori 2006, this issue). In the case of the 26 December 2004 earthquake, early results of inversions for fault slip patterns ranged widely. Some initial estimates included maximum slip values of only 6 m, whereas others obtained 20 m. Some of the variation reported occurred because resolution of slip is underdetermined, and these studies averaged slip over different fault areas. Months later, once the extremely-long-period GPS, geologic, and tsunami data were included in slip inversions, and once various plate interface dip angles had been tested, estimates of slip as large as 30 m were described over the largest-slip patch (Hirata et al. 2006), near the southeast end of the rupture zone, where

up to 18 m of slip occurred over an area of roughly 10,000 km^2 (Chlieh et al. 2006). Such high slip over such a large area produced the initial subevent, itself a potent seismic and tsunami source comprising the first third of the rupture, and precipitating the chain of subevents that dynamically extended the rupture length threefold alongstrike to complete the Sumatra-Andaman event rupture.

The total slip, both rapid and gradual, on the plate interface will probably remain the subject of many years of future study as inversion methods are further optimized and as additional data are collected. For example, longer GPS time series and future satellite imagery acquisitions over several years will help to clarify the pattern and amounts of postseismic deformation. Here, we summarize the current state of knowledge, with the expectation that the range of model results is a measure of the overall uncertainty caused by sparse data, imprecision of current methods, and the inherent inability to resolve an underdetermined problem. Much has been learned through the investigations summarized here; clearly some slip and afterslip features are well resolved by the data. A goal of this overview is to summarize all geologic and geodetic work published (or in some cases, in press or submitted) to date from all available sources. As such, the highlights selected from the diverse abundance of research results serve only as a pointer to a few of the many detailed studies accomplished through the efforts of others, some of which were surely inadvertently omitted from this overview.

GLOBAL CRUSTAL DEFORMATION AND SEISMIC HAZARDS

$M > 9$ earthquake sources have been among the most important sources of deadly and damaging historical tsunamis (e.g., Chile 1960, Alaska 1964, Sumatra-Andaman 2004). Through plate tectonics we understand and can quantify the motions of Earth's major and minor plates with respect to one another. We have recorded global earthquakes over the last century, and we find that seismic energy release occurs primarily along the boundaries where relative plate motions are concentrated. More recently, we have used space geodesy to measure plate motions so that we can observe not only sudden seismic energy release, but also the slow aseismic strain accumulation that directly leads to earthquakes, as well as the relaxation processes that follow them.

Taken all together, a reasonable basis now exists for characterizing and forecasting global seismic hazards and future earthquake potential. Consider two plates converging across a subduction zone (Figure 2). The surface across which they are in contact is the plate interface. Between megathrust earthquakes, strain accumulates and is measured geodetically. Areas of more rapid convergence around the world's convergent plate boundaries tend to have frequent large-to-great earthquakes and pose a generally greater seismic and tsunamigenic hazard (Figure 3).

Through work organized by the International Lithosphere Program (ILP), two major data products have been used in support of long-term earthquake forecasts: the Global Seismic Hazard Assessment Program (GSHAP) (http://www.seismo.ethz.ch/GSHAP/) and the Global Strain Rate Map (GSRM) (http://gsrm.unavco.org/).

Global seismic hazards have been mapped on the basis of historical earthquake activity (e.g., Pacheco and Sykes 1992), source characterization, and probabilistic seismic

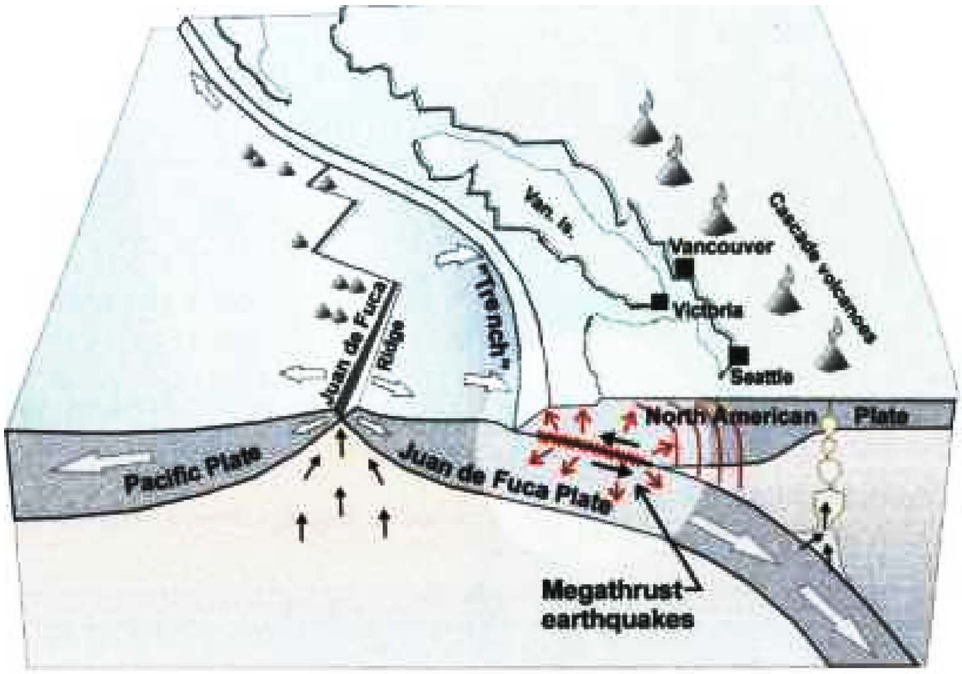

Figure 2. A subduction zone plate boundary. Where the downgoing and overriding plates are in contact, relative plate motion leads to strain accumulation that is then released in megathrust earthquakes that are typically tsunamigenic if $M > 9$ (source: Pacific Geosciences Center, Canada).

hazard analysis (PSHA) (e.g., Giardini et al. 1999, 2003; Shedlock et al. 2000). From GPS data the rates of crustal deformation, such as crustal convergence across subduction zones (Figure 4), are now also well known (e.g., Haines and Holt 1993; Kreemer et al. 2000a, 2003; Sella et al. 2002). Most recently, efforts to improve global earthquake hazard assessment have tried to improve the methods for including seismic catalog data (Bird and Kagan 2004).

Hazards from $M > 9$ class earthquakes are considerable along many of the world's subduction zones, and it is generally held that such events would be tsunamigenic. Less certain is whether or not smaller earthquakes, $9 > M > 8$, or even events below $M = 8$, would be likely to be tsunamigenic; some $8 > M > 7$ events were certainly tsunamigenic (e.g., Geist 1999).

UNANTICIPATED EARTHQUAKE AND TSUNAMI

For some portions of the world's plate boundaries, there exists no easy consensus regarding either seismic or tsunamigenic potential. Although not as frequent as Pacific Ocean tsunamis, Indian Ocean tsunamis during historical time have included the devastating tsunami example associated with the eruption of Krakatoa (27 August 1883). The

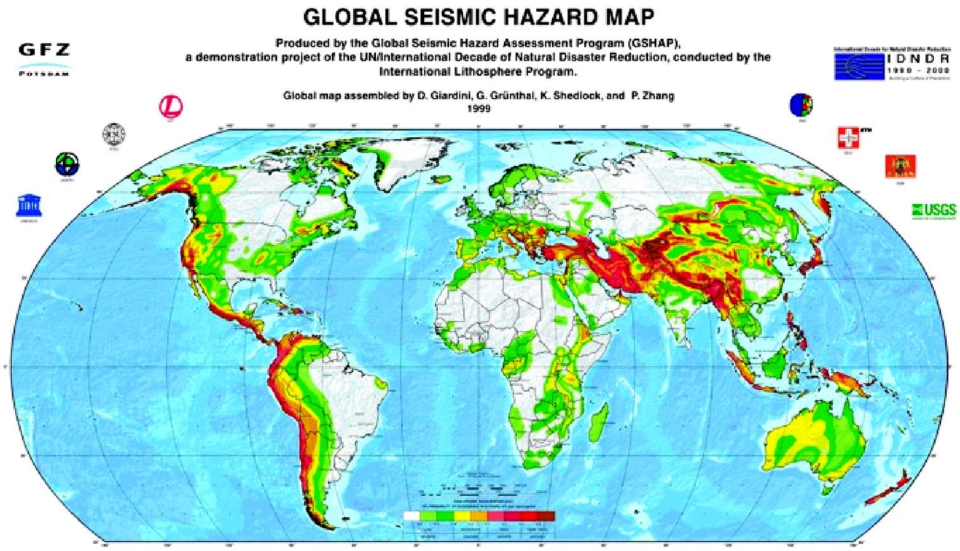

Figure 3. Global Seismic Hazard Map. From the global earthquake catalog, seismic source characterization, strong motions and PSHA, GSHAP compiled this map (source: GSHAP by Giardini et al., 2003, for the ILP).

seismic hazard of subduction zones along the Indian Ocean margin off Sumatra had, for many years, been recognized to be high (e.g., Giardini et al. 1999, 2003; Shedlock et al. 2000). From GPS data, the rate of crustal convergence was known to be appreciable, and it was clear that strain accumulation was occurring across the megathrust along Sumatra and Java (e.g., Haines and Holt 1993; Kreemer et al. 2000a, b). The historic and prehistoric sequence of great events along the subduction zone from the study of historical records and fossil evidence from corals showed a high risk of a repeat of an $M \approx 9$ tsunamigenic earthquake from just south of the Batu Islands to the southeast, similar to an event pair that had struck in 1797 and 1833 (Newcomb and McCann 1987, Zachariasen et al. 1999, Natawidjaja et al. 2006). The hazard from an $M \approx 9$ class great earthquake was considered highly likely in even the most recent probabilistic seismic forecasts (e.g., Petersen et al. 2004), and it was also generally held that such an event would be likely to be tsunamigenic.

Missing, however, was an appreciation for the earthquake and tsunami hazard from north of the island of Sumatra. As quoted more fully in the Introduction, McCann et al. (1979) had stated what became the accepted idea: there did "not appear to be great earthquakes associated with the Sunda arc in the Andaman-Nicobar region." Because the direction of plate convergence becomes highly oblique northward from 3° N (e.g., McCaffrey et al. 2000), and because strike-slip motion is being accommodated on the Great Sumatra and Andaman faults, for example, it was generally believed that the efficiency of fault-relative movement across the plate interface was being resolved into fault-normal and fault-perpendicular components (termed *slip partitioning*) in such a way that

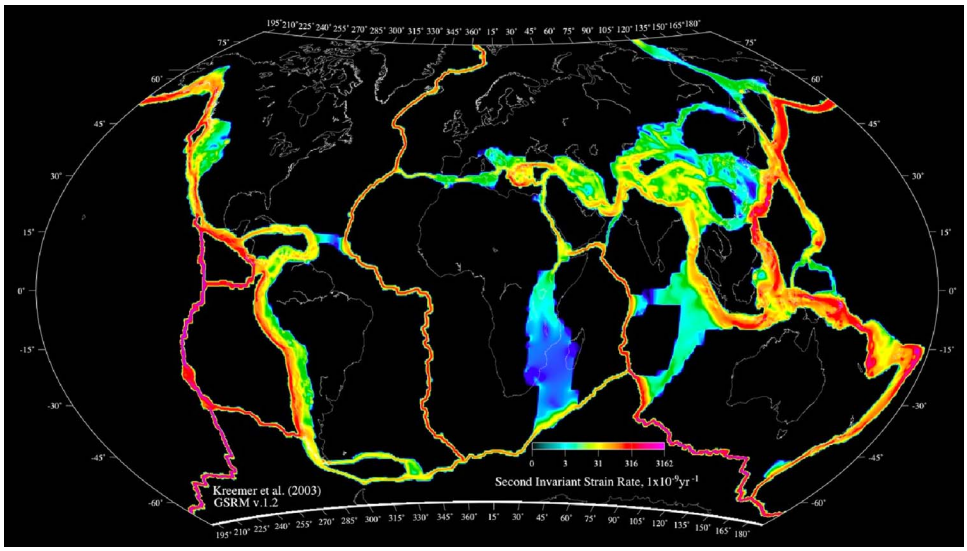

Figure 4. Global Strain Rate Map. From global space geodesy (e.g., GPS) station velocity measurements as well as other data, the GSRM group compiled this map showing relative plate motions (source: GSRM by Kreemer et al., 2003, for the ILP).

the trench-normal convergent component was slight or negligible (Prawirodirjo et al. 1997, Genrich et al. 2000, McCaffrey et al. 2000).

A significant change in tectonic setting, however, occurs at about 10° N, midway up the Nicobar-Andaman island chain (between Car Nicobar and Little Andaman islands). Here, the ridge-transform system beneath the Andaman Sea (the purple line in Figure 1) abuts and interacts within the back-arc of the subduction zone (Curray 2005). Along the arc, variations in the sediment thickness and age of the subducting plate may also help to determine the change in coupling across the plate interface (e.g., Chlieh et al. 2006). As a result, oblique convergence of 14±4 mm/year occurs. This had been detected at Port Blair (at 12° N in Figure 1), between the Andaman plate and Indian plate (Paul et al. 2001, Bilham 2005). A crucial point, however, hinges on the pole of rotation for India, recently estimated by both Bettinelli et al. (2006) and Socquet et al. (2006), and the relative motion of the Capricorn plate (DeMets et al. 2005). Thus the former assumption, that trench-normal convergence was negligible through the Andaman Islands, was in the midst of gradually being disproved by using GPS at about the time the event happened.

Little is known even now about the northern extent of the seismic and tsunami hazard, although early historical records are being searched for evidence of events off Myanmar. Evidently, slip in the 2004 Sumatra-Andaman event extended as far north as Preparis Island at 14.9° N (Meltzner et al. 2006). Although it is conceivable that seismic and tsunami hazards could have been more clearly recognized and characterized for the con-

vergence across the plate boundary from ~10° N to the northern extreme end, the interseismic deformation in this area remains unclear even with the benefit of hindsight.

Hence, before this event occurred, no one had ever argued for the possibility of an $M \approx 9$ rupture extending northward through the Andaman and Nicobar (A&N) Islands. In that sense, the northernmost 800 km of this earthquake rupture was completely unanticipated. Furthermore, that at least the southern half of this portion of the rupture was tsunamigenic meant widespread damage from inundation in areas of Thailand, Myanmar, Sri Lanka, and India that would simply not have been included in tsunami hazard models prior to this event. Because there was not thought to be as great a seismic threat from the subduction zone north of 6° N and up to 11° N, there was thought to be a relatively low tsunami threat to these coastlines that ended up being very heavily damaged in 2004.

Hypothetically, this does not need to have been the case. Had there been an array of continuous GPS stations operating for several years, better constraints on the seismic hazards would certainly have been possible. Furthermore, had investigators been able to sample corals in this region, as had been done off Sumatra, the paleoearthquake history would certainly also have helped in quantifying hazards for this section of the subduction zone. Systematic searches for paleotsunami deposits could have been conducted regionally as well. Such studies here, or elsewhere, can be generally beneficial for quantifying earthquake and tsunami hazards. As an added benefit, these studies and monitoring arrays will then also provide valuable data after future great earthquakes.

A direct lesson taught, by this example, has been applied in the similar case of the westernmost extreme Aleutian archipelago. Similar in its oblique plate motion to this section of the A&N Islands, it had also previously been thought to have a low seismic and tsunami hazard. Now, however, revisions are being made to accept the possibility of an $M \approx 9$ event rupturing this area with large slip. In a few other cases worldwide—for example, the Ryukyu, South Sandwich, and Caribbean archipelagos—similar revisions are being considered. Even where trench-normal convergence rates are low, hazards exist and need to be carefully re-evaluated on a case-by-case basis using the best available geodetic, paleoseismic, paleotsunami, and other data.

Another lesson gained from the 2004 megathrust rupture is that segments that were not thought likely to rupture together now should be taken into account as a finite probability. That is, where historical or paleoseismic evidence suggests $M \approx 8$ class events but no $M \approx 9$ class events, the possibility of $M \approx 9$ class events cascading through multiple-segment ruptures needs to be appropriately considered. This new information is now being utilized in revising global earthquake hazard models and in modeling tsunami potential hazards for the western Pacific region (source characterization work in progress by NOAA and USGS).

THE 26 DECEMBER 2004 SUMATRA-ANDAMAN EARTHQUAKE

In simplest terms, the rupture began at 3.0° N off the northwestern end of Simeulue Island on the plate interface megathrust fault. The early onset or first stage of rupture led to rapid large slip unilaterally toward the north, producing a large slip patch of some

20 m of slip across the downdip width for several hundred kilometers alongstrike. Rupture then continued northward and began to slow down until gradually stopping at about 15° N. Along the way, several additional large slip patches occurred, but none were as large as the initial one. The character of rupture is thought to have changed most distinctly upon passing into the different tectonic regime north of 10° N; after this, it slowed down to the point that it clearly was no longer producing a tsunami from 11° N to 15° N (Geist et al. 2006). Although many early models included this northern reach in their tsunami sources, some water level gauge data have been shown to be inconsistent with this portion of the rupture being tsunamigenic (Neetu et al. 2005). The following sections review the observations in more detail.

GEOLOGICAL OBSERVATIONS

For great continental earthquakes, primary evidence of faulting can be documented by directly mapping fault surface ruptures, and slip on the fault is observed by measuring offset features. In this case, however, because the earthquake occurred along the megathrust plate interface, the rupture is believed to have broken the seafloor along the Sunda Trench in water depths of about 3–5 km along the arc where it cannot be readily observed. For this reason, geological studies rely for the most part on secondary observations of deformation associated with the megathrust rupture and slip on the buried plate interface.

In one place called the "Ditch," however, exploration by the Sumatra earthquake and tsunami offshore survey (SEATOS) cruise found disruption of the seafloor surface that was interpreted as faulting at the seafloor along the trench (Moran and Tappin 2006). The researchers described this as a linear depression at the toe of the deformation front, suggesting evidence for recent seafloor movement. The evidence, however, is not clearly indicative of primary tectonic offset along the seafloor outcrop of the megathrust fault (Henstock et al. 2006). Instead, an east-facing striated scarp along the western edge of the Ditch with a height of up to 12 m of vertical separation was found. This apparently tectonic scarp along the frontal thrust ridge is the only potentially primary geological evidence of the seafloor rupture reported so far (Figure 5). Henstock et al. (2006) show several possible interpretations of this feature, none of which is a simple seafloor rupture of the primary megathrust fault plane. Instead, they argue that folding and backthrusting at the deformation front pervade the structural style alongstrike. Future cruises can be expected to obtain more extensive observations of seafloor faulting and deformation with new deep-ocean manned and unmanned submersibles and imaging technologies.

Where rupture occurred at great depth beneath the islands off Sumatra and along the A&N Island groups, secondary geological evidence of slip on the plate interface was often expressed as dramatic uplift (Figures 6 and 7) or subsidence (Figure 7). Coral reefs, marshlands, estuaries, and mangrove swamps, as well as docks and other harbor facilities in populated areas, were stranded well above pre-event high tide lines, while in other places coral reefs were submerged or towns were flooded. In some cases, uplifted villages benefited from being raised coseismically just prior to inundation by what would probably otherwise have been a damaging tsunami.

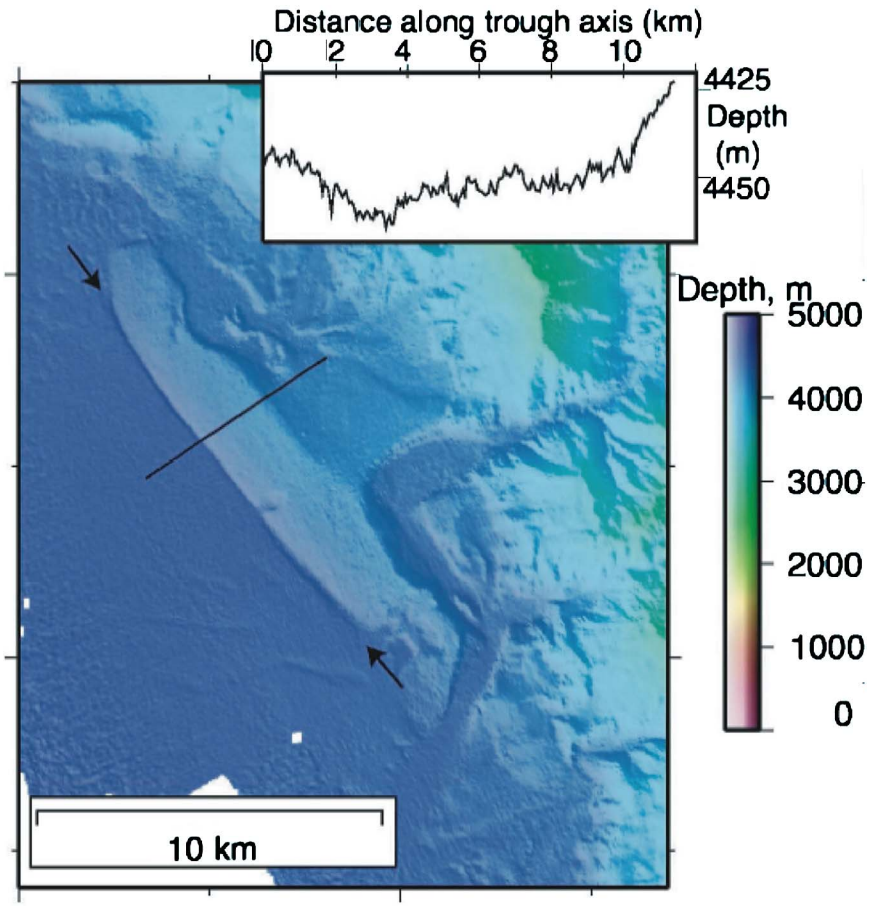

Figure 5. Possible primary evidence of seafloor faulting at the trench was obtained by a remotely operated deep submersible at a water depth of 4.4 km (Moran and Tappin 2006). This feature and sense of motion, however, are more consistent with fault slip on a backthrust (Henstock et al. 2006), and the deformation is not concentrated on a single, simple fault scarp.

Although a short-term benefit, this uplift has proved to be a long-term problem for residents. At Sirombu, on the central west coast of Nias, uplift of 2.6 m had the following effects: the town pier was lifted high and dry and has been rendered useless; the harbor is now too shallow for large boats, and medium boats cannot get close enough to shore; villagers must now walk several hundred meters several times per day going back and forth across the dry reefs to reach the ocean. Long-term effects of subsidence at other locations include flooding of villages at high tides and landward beach erosion into villages and coconut plantations (Meltzner 2006).

Comprehensive studies of uplift and subsidence throughout the region were made possible through novel uses of spaceborne imagery (Meltzner et al. 2006, Tobita et al.

Figure 6. Uplifted coral reef, photographed from an Indian Coast Guard helicopter on 28 December 2004 at North Sentinel Island (Nambath 2005). The uplift is estimated to be 1–2 m (Bilham et al. 2005). This island is home to the Sentinalese, one of the world's few remaining largely untouched native people, who are said to shoot arrows at those who approach the island. Evidently, this helicopter was fired upon by a lone Sentinalese (according to the report that accompanied this photo).

2006). Tobita et al. (2006) observed changes in synthetic aperture radar (SAR) backscatter intensities in order to map uplifted and submerged areas. To do so, they differenced shorelines estimated from before and after imagery. Seaward shifts of the shoreline indicated uplift, whereas shoreward shifts indicated subsidence. Such information was compiled for the entire rupture length.

By carefully correcting satellite imagery for tidal stage at the times of pre-event and post-event advanced spaceborne thermal emission and reflection (ASTER) radiometer imagery acquisition, Meltzner et al. (2006) were able to place minimum bounds on either uplift or subsidence at each of 160 imagery analysis sites. Field observations of uplift and subsidence were also made at 10 sites, and vertical deformation measurements reported elsewhere were evaluated and compiled. The Meltzner et al. (2006) study showed that uplift extended along the total length of fault rupture from ~2.5° N (on Simeulue Island) to ~14.9° N (on Preparis Island), a total of approximately 1,600 km.

While the datum at Preparis Island is considered less robust than other data in the study, Meltzner et al. (2006) concluded that rupture did extend nearly to 15° N, which is about 100 km farther north than any other studies had estimated, 300 km longer than the estimated 1,300 km that has been widely stated (e.g., Bilham 2005), and 600 km longer

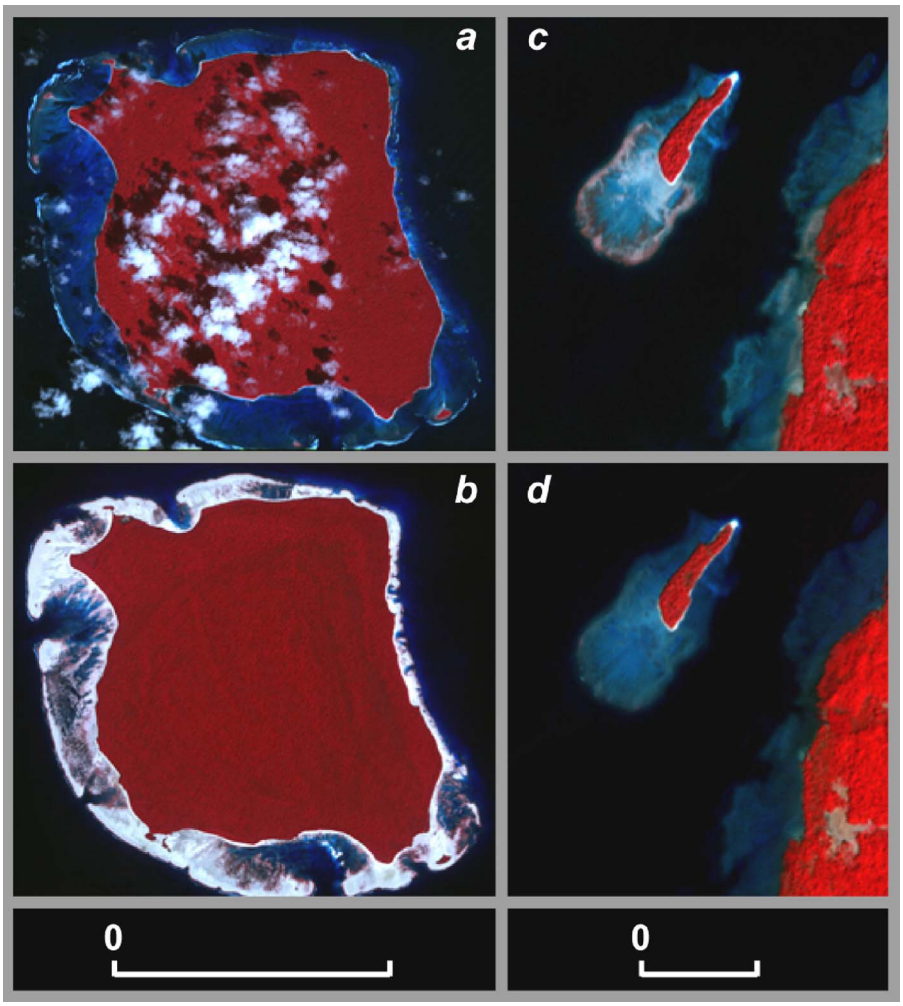

Figure 7. (a) Pre-earthquake and (b) post-earthquake ASTER images of North Sentinel Island, showing emergence of the coral reef surrounding the island. (c) Pre-earthquake and (d) post-earthquake ASTER images of a small island off the northwest coast of Rutland Island, 38 km east of North Sentinel Island, showing submergence of the coral reef surrounding the island. The "pivot line" must run between North Sentinel and Rutland islands. Note that the scale for the North Sentinel Island images differs from that for the Rutland Island images. Scale bars as follows: (a) and (b) 0–6 km; (c) and (d) 0–1 km. (ASTER images courtesy of NASA/JPL from Meltzner et al., 2006).

than initially estimated by seismologists (e.g., Lay et al. 2005). Furthermore, the "pivot line" between uplift and subsidence was identified alongstrike of the rupture, providing a strong constraint on the downdip edge of slip on the megathrust plate interface. The arc-normal distance from the trench to the pivot line varied from 80 to 120 km, placing

an important constraint on rupture width along the strike of the entire rupture. This general rule will vary with factors such as downdip skewness and alongstrike variation of the actual slip distribution. Some studies estimate the total downdip rupture width to be greater, perhaps 240 km, in the southeastern portion of the rupture, narrowing to 160–170 km in the northern two-thirds of the rupture (Lay et al. 2005).

The Meltzner et al. (2006) study defined the overall rupture dimensions and outline and quantified the northernmost half to two-thirds of the rupture, where the initial propagation was evidently followed by gradual large slip and therefore was ambiguously recorded by seismological data. This study not only complemented seismology, which was especially good at imaging the rapid slip within the southern portions of the rupture, but it also complemented GPS geodesy. Because this new remote-sensing method provided far greater spatial detail, it allowed the pivot line to be precisely located alongstrike, and in two cases may have actually provided a more reliable measure of vertical deformation than the survey-mode GPS data.

GEODETIC OBSERVATIONS

Most available space geodetic high-accuracy measurements of deformation associated with the Sumatra-Andaman earthquake are from several vital sources of GPS data (as compiled in Figure 8): (1) the International GPS Service (IGS), as has been extensively described (Banerjee et al. 2005, Vigny et al. 2005, Kreemer et al. 2006); (2) national Malay and Thai GPS array data from the Department for Survey and Mapping Malaysia and Royal Thai Survey Department, as reported by Vigny et al. (2005); (3) National Coordination Agency for Surveys and Mapping Indonesia (BAKOSURTANAL) data from Indonesia, as reported primarily by Subarya et al. (2006); and (4) the Survey of India (Gahalaut et al. 2006) and other GPS sites (Jade et al. 2005) along the full extent of the A&N Islands.

A handful of continuously operating GPS stations fortuitously captured this event at close-to-intermediate-distance ranges, while the entire global GPS network recorded this event (Banerjee et al. 2005, Kreemer et al. 2006, Hashimoto et al. 2006). “No point on Earth remained undisturbed at the centimeter level,” said Bilham (2005). Even at Earth’s gravest modes of free oscillation, space geodetic data supported insights that would not have been possible with seismological instrumentation alone (Banerjee et al. 2005, Kreemer et al. 2006).

No other great earthquake had ever previously been captured by such an array of extremely-long-period instrumentation, as well as with the comprehensive before-and-after high-resolution and hyperspectral satellite imagery. For this reason, much has been learned about the final two-thirds of the rupture process and about slow “infraseismic” slip on the plate interface. The geological and geodetic data collected have extended the range of our knowledge about the earthquake source into ultra-long-period and super-slow motion. As the image of the rupture process becomes clearer with improved modeling in the future, these results can be expected to have an important impact on our understanding of earthquake source physics and dynamic friction in spontaneous rupture modeling.

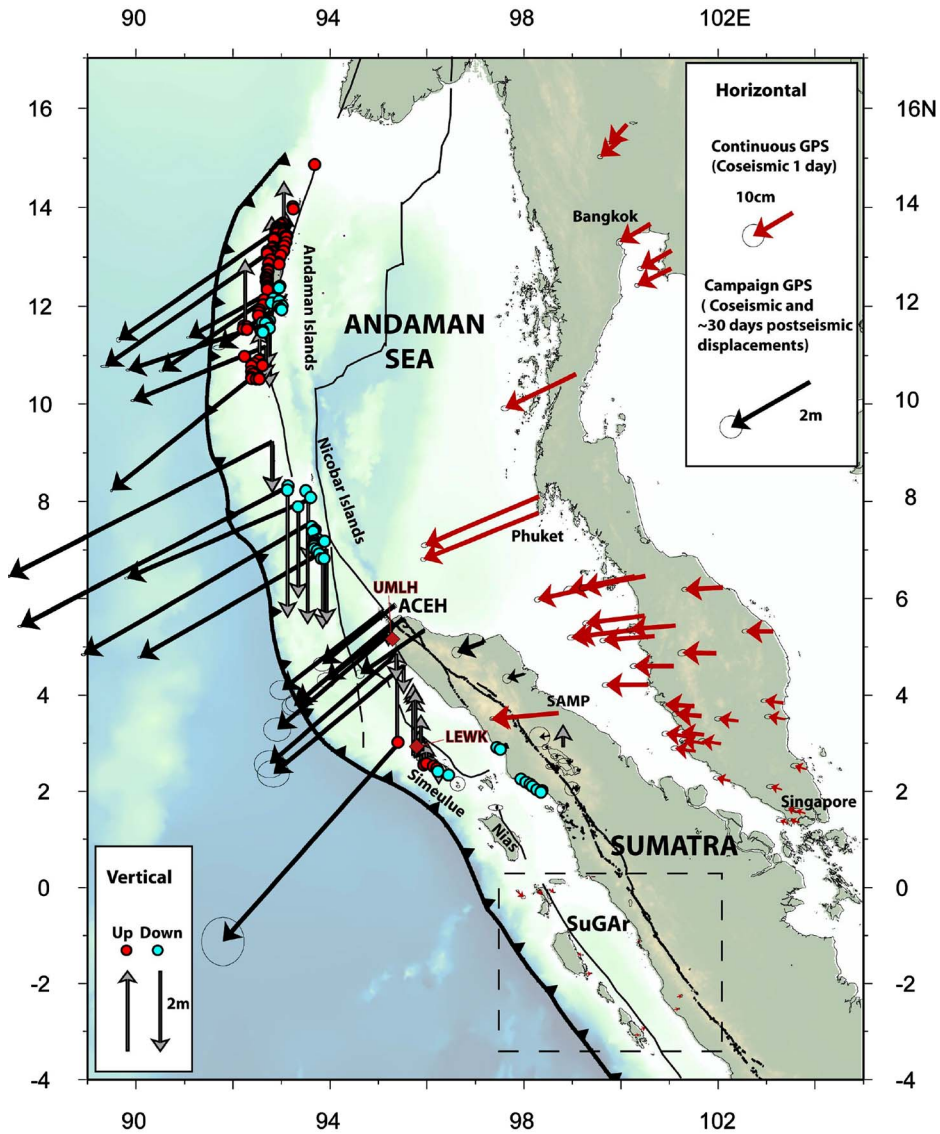

Figure 8. Summary of all geodetic and geological deformation data for the 2004 Sumatra-Andaman earthquake; red (in grayscale: dark) and blue (in grayscale: light) dots summarize data from Meltzner et al. (2006), red (in grayscale: gray) arrows are continuous GPS (Vigny et al. 2005), and black arrows are campaign-mode GPS (Subarya et al. 2006, Gahalaut et al. 2006). The array of continuous GPS stations that recorded the Nias-Simeulue event, called SuGAr (for Sumatra GPS array), is indicated by a dashed box (modified from Chlieh et al., 2006).

MERGING SEISMIC, GEODETIC, AND GEOLOGIC DATA

Judging from all studies, it seems that the northward propagation of rupture was rapid enough to radiate some seismic energy along most of the way (e.g., Ammon et al. 2005, Guilbert et al. 2005), but perhaps anomalously slow in the northernmost reaches of the rupture (e.g., Bilham 2005). Evidently, at least some small amount of slip made its way rapidly nearly to the northern end, otherwise there would have been no high-frequency T-wave radiation (Guilbert et al. 2005). Perhaps initially only a small amount of slip occurred, followed by slowly increasing slip, or slow updip (or downdip) propagation (Figure 11). The geological and geodetic data available indicate large total slip, even in the northern reaches (Meltzner et al. 2006, Gahalaut et al. 2006, Subarya et al. 2006, Chlieh et al. 2006), but it may never be clear how that slip evolved with time. In any case, evidently this northern portion of the rupture, from either ~9° N (Lay et al. 2005) or ~11° N (Neetu et al. 2005) to the northern extreme end, did not excite much tsunami energy (Geist et al. 2006).

An interesting possibility is that a small amount of rapid slip was followed soon afterwards by a large amount of rapid afterslip, perhaps indicating slower-than-normal healing after the rupture front passed. Slow healing could occur because of an alongstrike change in frictional properties, resulting from the older subducting plate and greater sediment thickness in the north, for example. These differences from south to north could cause a lower effective coupling as the rupture propagated north. Rupture may also have switched into a different mode of crack propagation as it went to the north, in such a way that the slip direction rotated from being parallel to the rupture propagation direction to being perpendicular to it, as was seen for the Chi Chi earthquake (e.g., Ji et al. 2003, Aagaard et al. 2004). The combined effects of restrengthening and rotation to updip instead of alongstrike rupture direction may have gradually arrested the rupture. Such speculations are not supported by the data at present, but they are suggested in hopes of motivating further study of these important aspects of the rupture process and the implications for earthquake source physics.

A challenge has been evident throughout the sequence of papers that attempt to describe the source properties of this great earthquake. Some papers have chosen to present multiple models based on the same data set, or on different subsets of data. The event defied many early attempts to quantify it, yet as more data have become available, a clearer picture is emerging. Rather than reviewing the incremental progress of steps that have led to the currently best available model, we will focus directly on this model alone for both coseismic and postseismic deformation associated with the earthquake. This model (Figure 9) by Chlieh et al. (2006) has included all available deformation data from all sources, and the researchers have done a careful and rigorous job of fitting all the data. Most features of the model are well resolved or are explained as being underdetermined within their paper. At least one other similarly detailed modeling study also merges all available data to form a comprehensive source model (Banerjee et al. 2006), and as new data and methods become available, further modeling will surely be the subject of many future studies to refine our understanding of this earthquake's source process.

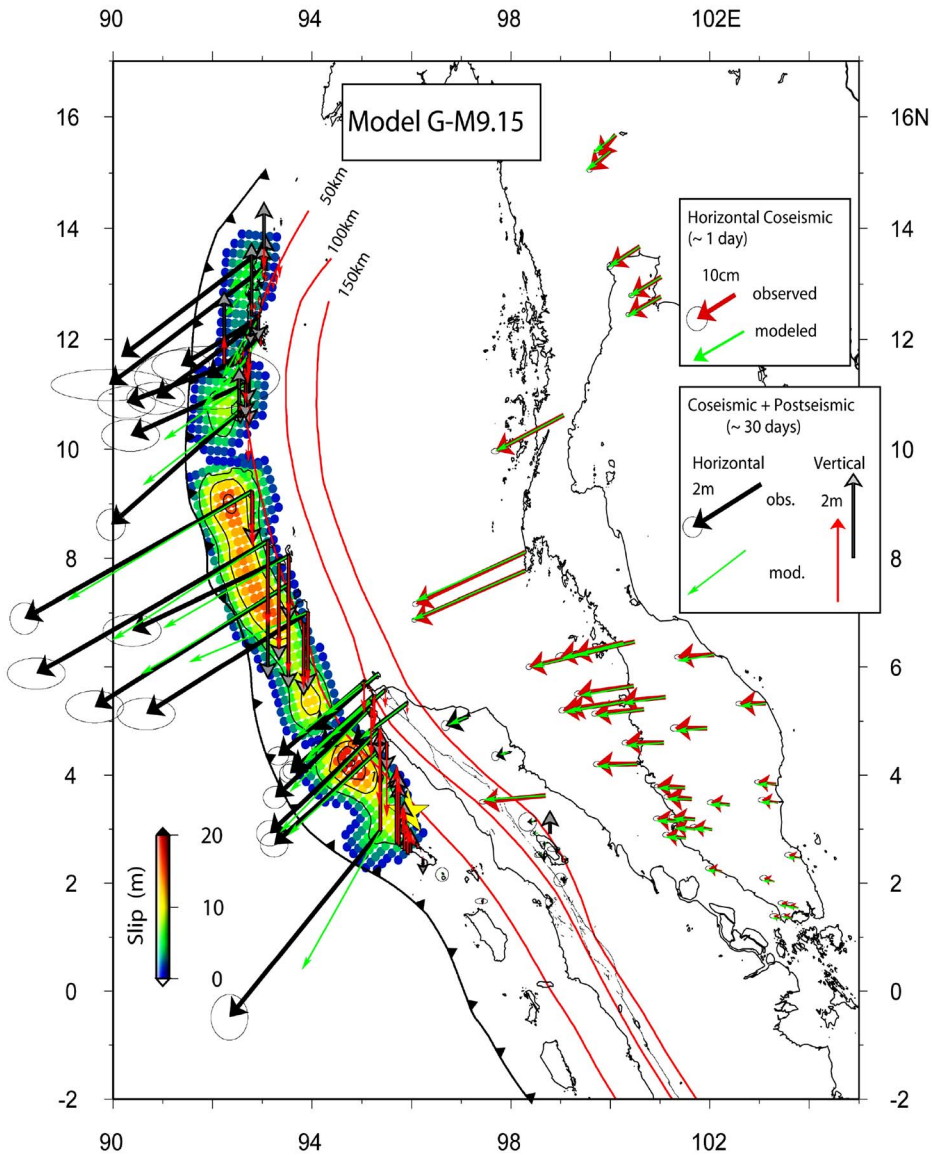

Figure 9. Slip distribution, with predicted displacements (green vectors; in grayscale: light gray) for the preferred coseismic model G-M9.15 (Chlieh et al. 2006). Coseismic displacements (red vectors; in grayscale: darker gray) show displacements measured the day after the earthquake (Vigny et al. 2005). Near-field displacements (black vectors) include coseismic deformation and 20–40 days of postseismic deformation (from Chlieh et al., 2006).

Seismological data are best for resolving the rise time and slip evolution as rupture propagates, as well as for resolving slip (even at the deepest portions of the fault) within the initial several hundred seconds of a rupture. The geodetic and geologic data are best for resolving the overall geometry and outline of the rupture, resolving the final slip pattern (including immediate and short-term postseismic deformation), and providing an independent set of observations that may be used to help evaluate competing seismic or tsunami models that used other data as input. In general, the most satisfactory models are ones that can be used to reproduce all of the particular independent data sets.

For example, if one produces a model based purely on seismological data and then computes synthetic static displacements at the GPS site locations, one should expect to fit the independent GPS observations adequately, and vice versa. Either a strictly seismic or geodetic model can be expected to provide a good simulation of tsunami observational data or free oscillation recordings, and so on. We have reached a point with sufficient data for this earthquake that now these cross-validations are working much better than they were at first. In fact, Chlieh et al. (2006) go to great lengths to demonstrate to the reader that each of their models, using one type of data at a time, do not badly violate any of the independent data sets. They then produce a single preferred model in which all available data are jointly inverted, using appropriate weighting functions. This result is shown in Figure 9, a model that fits all currently available observations remarkably well.

Interestingly, deep afterslip patterns fit in neatly downdip from each of the two largest coseismic slip patches (Figure 10). This follows Scholz's (2002) concept of rate-strengthening behavior below what he terms the lower stability transition at depth. That is, in this model, the large slip within the brittle portion of the plate interface placed high strains downdip that could not be relieved instantly, driving a nonlinear response within the normally plastic flow regime and producing a transient creep pulse that probably propagated downdip away from the highest-slip areas.

Because the available continuous GPS data are sparse and sporadic for the Sumatra-Andaman event, and because the post-event geologic and geodetic data were collected over a long time span, relatively broad discrete time windows for showing the progression of deformation throughout the postseismic slip are used (e.g., Chlieh et al. 2006). Even so, it is evident that postseismic slip migrated in time and space in an intriguing manner. Unfortunately, details of the evolution of postseismic slip were not observed, due to the lack of continuous GPS stations above or very near the rupture patch. Furthermore, the available data may be alternatively modeled as asthenosphere relaxation (Pollitz et al. 2006a, Banerjee et al. 2006).

A summary of coseismic and postseismic results, overlaid with an illustration of high-frequency seismic energy radiation, as well as the aftershock distribution, is shown in Figure 11. In general, excellent agreement has been found between the two estimated coseismic models shown, except that between 6.5° N and 9.5° N the geodetic data indicate larger coseismic slip than the seismic data alone. Interestingly, the two geodetic model slip peaks within this section of the fault, however, do correspond to larger radiated T waves (Guilbert et al. 2005). For most of the rupture's length, coseismic slip and afterslip are proportional; that is, where coseismic slip was large, the postseismic slip is

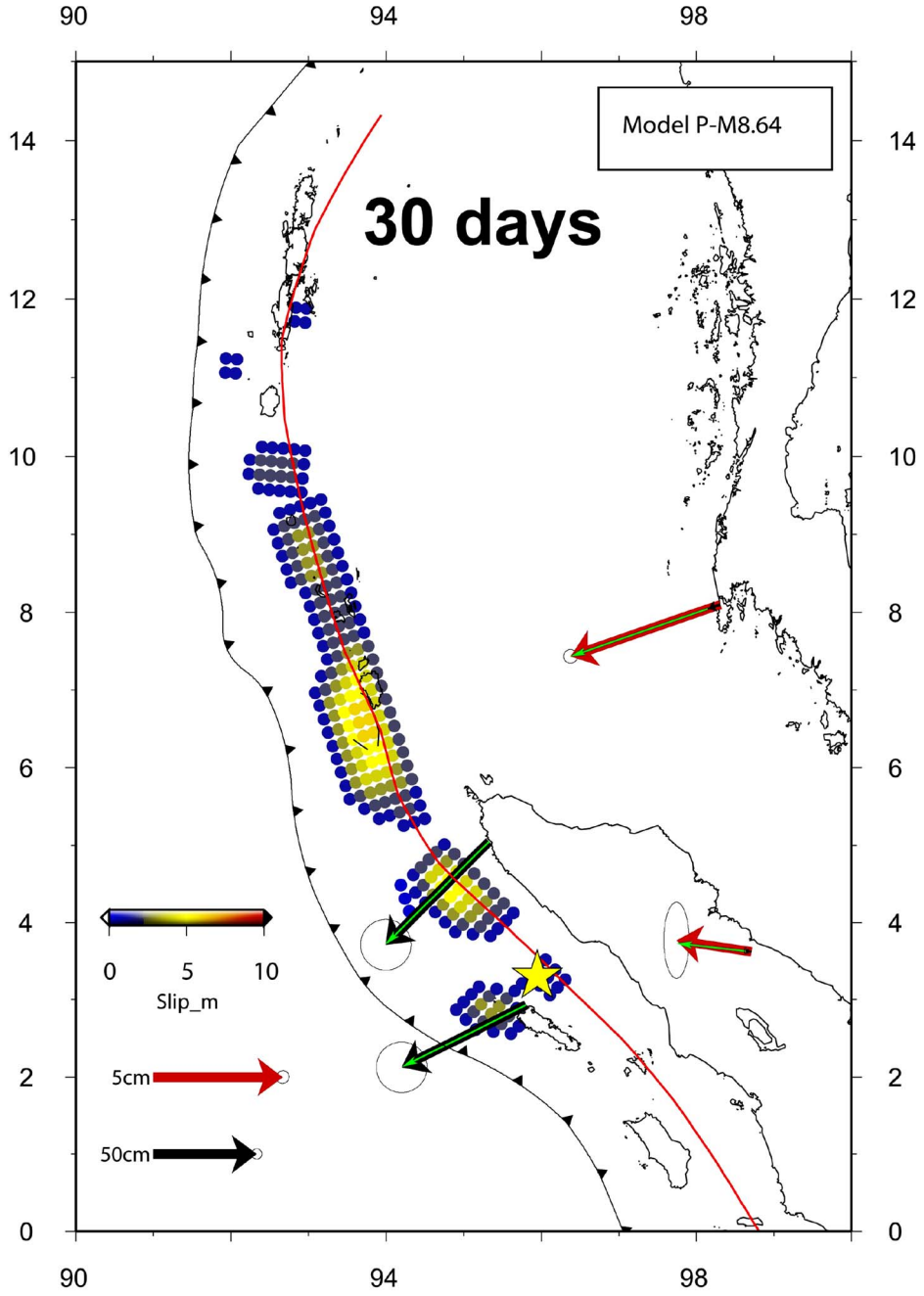

Figure 10. Postseismic slip resolved on the plate interface. The inversion result uses the model of Perfettini and Avouac (2004) to fit the one month of postseismic horizontal displacements recorded at Medan, Phuket, Ujung Muloh, and Lewak of the SuGAr (from Chlieh et al., 2006; data courtesy of Caltech Tectonic Observatory).

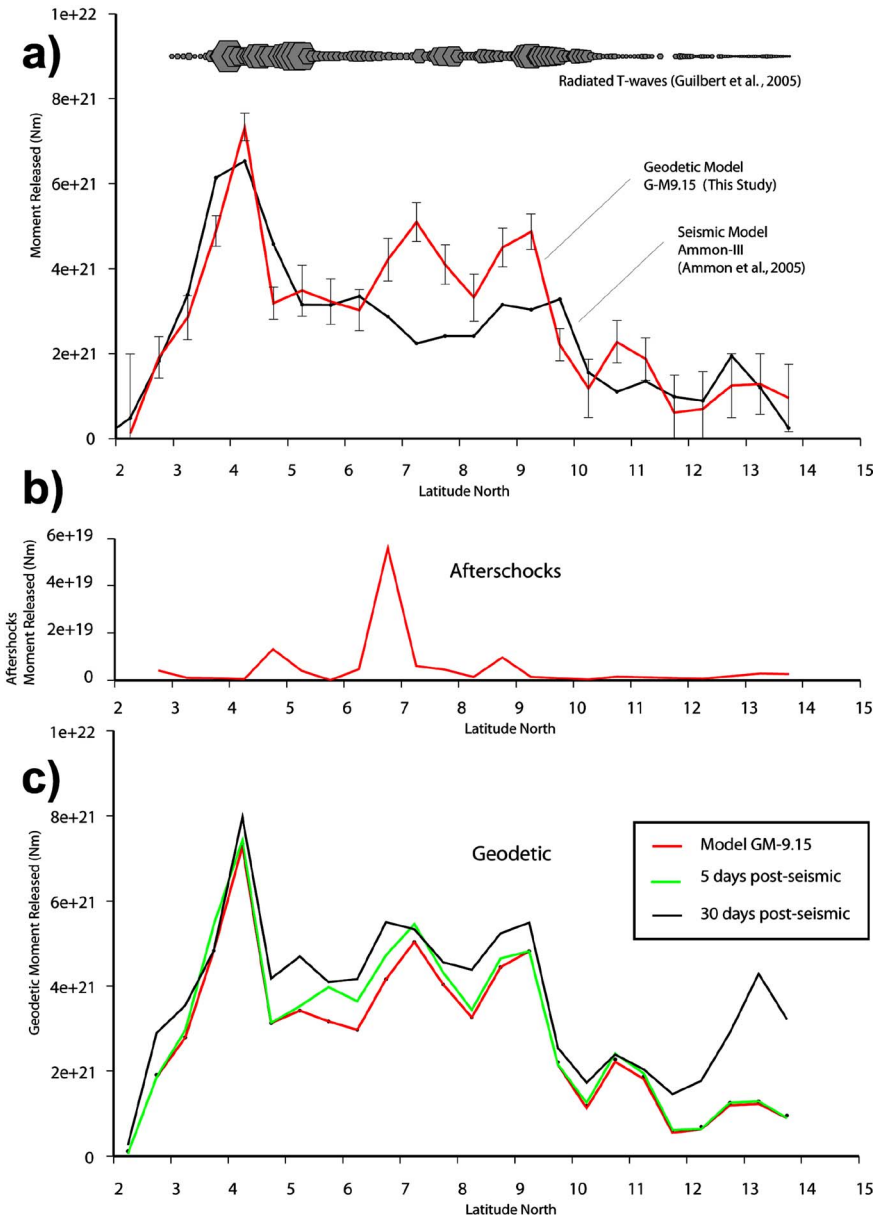

Figure 11. (a) Coseismic moment release alongstrike, estimated by seismological and geodetic methods and showing T-wave energy radiation across the top. (b) Moment contribution of aftershocks alongstrike. (c) Comparison of coseismic and postseismic moment release alongstrike, showing 5-day and 30-day progression of afterslip (from Chlieh et al., 2006). While it had been generally agreed that the tsunamigenic portion of the rupture extended only to ~9 ° N (Lay et al. 2005), recent tide gauge data indicate that tsunamigenic rupture continued to 11° N (Neetu et al. 2005) and that significant total slip extended past 14° N and perhaps even to 15° N (Meltzner et al. 2006).

also large. In the northern part, from 12° N to 14° N, however, afterslip is very large compared with coseismic slip. This generally corresponds to the section of the fault that is thought to have coupled less energy into the tsunami (e.g., Geist et al. 2006). Bilham (2005) suggested only slow slip in about this same section of the fault, yet more recent work has indicated that at least some early-onset rapid slip also occurred here. A way to reconcile these ideas has been suggested above in this paper.

As shown by Meltzner et al. (2006), the coseismic downdip extent is marked by the pivot line, which generally falls along the island arc in this case. Therefore, populated areas along the arc were particularly well located to detect postseismic variations in subtle uplift and subsidence effects that indicate the postseismic transition to slip being concentrated deeper on the plate interface. In general, the postseismic model predicts that the pivot line will systematically shift away from the trench, since the focus of afterslip is deeper than the coseismic focus.

This has been tentatively noted at Port Blair in the Andaman Islands (Gahalaut et al. 2006), and possibly elsewhere (Bilham 2006), although continuing observations are needed to be certain. Data collected at Port Blair include GPS observations, water level data, photos taken at different times, and personal accounts. After the coseismic slip, the town was submerged in 1–2 m of water and flooded; it is situated to the east of the pivot line. During the postseismic interval, as slip on the plate interface deepens, the pivot line can be expected to migrate eastward and away from the trench, so Port Blair might be expected to rebound through time and begin uplifting and even re-emerging in the future. Further interesting details of observations at Port Blair, including historical and geological accounts of long-term vertical motions in these islands, are given by Bilham et al. (2005). GPS data and water level records from the 2004 event have recently been published (Bilham et al. 2005, Neetu et al. 2005, Gahalaut et al. 2006), possibly indicating some vertical postseismic rebound and the predicted reversal from coseismic subsidence to postseismic uplift (Gahalaut et al. 2006). Evidence collected more recently supports systematic reversals between coseismic and postseismic vertical motions throughout the A&N Islands, with postseismic motions about 10–15% of the coseismic amounts (Bilham 2006).

One place where this pivot line migration would probably be most noticeable, if the coseismic and postseismic models of Chlieh et al. (2006) are correct, is at the Indira Point lighthouse at the southern tip of Great Nicobar. Here, the earliest report of subsidence was given as 4.25 m. Later reports re-estimated subsidence at only 1.4–1.5 m, as summarized by Bilham et al. (2005). Unfortunately, it is not clear whether there was a problem with units (e.g., possibly measured in feet, but erroneously reported as meters). This discrepancy in the observations, if confirmed through further field studies, GPS observations, and remote sensing investigations, may be best explained by coseismic subsidence of over 4 m, followed by postseismic uplift in the ensuing weeks of ~2.5 m due to deep aseismic slip on the plate interface. A similar reversal was observed, for example, after other large ($M \approx 8$) subduction events such as the 1995

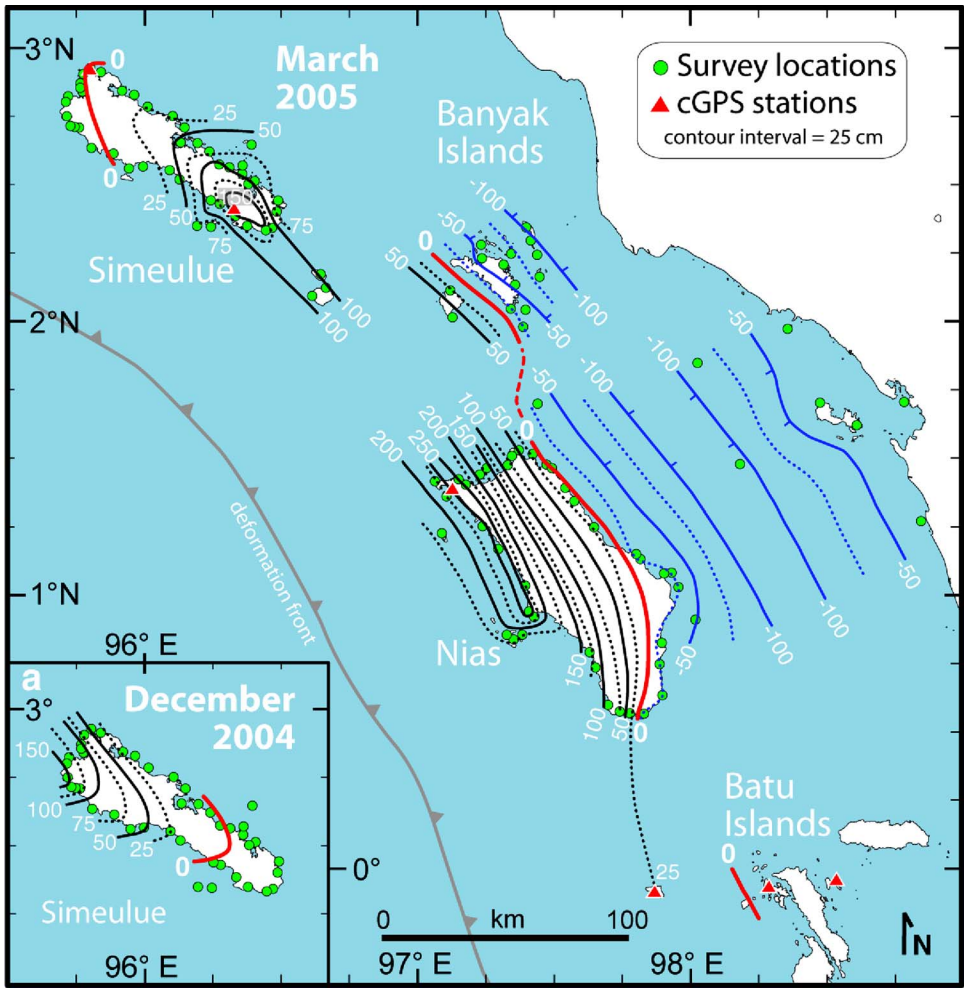

Figure 12. Contour maps of vertical deformation during the December 2004 Sumatra-Andaman (see inset) and March 2005 Nias-Simeulue earthquakes (in cm). Red (in grayscale: light gray) contours show uplift, and blue (in grayscale: darker gray) contours show subsidence. The white contour shows the pivot line demarcating the boundary between uplift and subsidence (e.g., Meltzner et al. 2006). Solid contours are at 50-cm intervals, and dashed contours are at 25-cm intervals (modified from Briggs et al., 2006).

Jalisco, Mexico earthquake (e.g., Melbourne et al. 1997, 2002). These observed reversals presumably result from the same physical process of deep aseismic creep, accommodated by plastic deformation of mineral crystals within the deep-seated shear zone beneath the downdip edge of megathrust coseismic rupture (Scholz 2002).

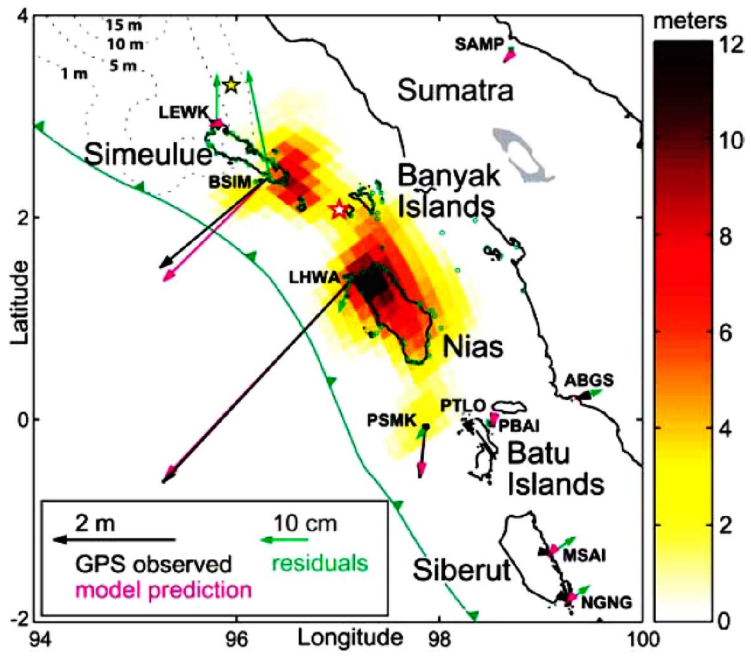

Figure 13. Modeled coseismic slip for the 28 March 2005 Nias-Simeulue rupture. Displacements from GPS are in black, model values are in pink (in grayscale: medium gray), and model residuals are green (in grayscale: lighter gray) vectors (note the change of scale). The slip reached 8 m under Simeulue and 11 m under Nias. The epicenter of the March 2005 main shock is shown by a large star, and the green (in grayscale: light gray) line denotes the position of the Sunda trench. Dashed contours show modeled slip for the 2004 Aceh-Andaman rupture, and the smaller star denotes the 2004 epicenter (Briggs et al. 2006; from Hsu et al., 2006).

THE 28 MARCH 2005 NIAS-SIMEULUE EARTHQUAKE

While the Sumatra-Andaman event was unusually large, with a very-long-duration source, it was sparsely recorded instrumentally in the near field. In contrast, the Nias-Simeulue event was relatively well observed. Prevalence of a particular coral genus, called *Porites*, within the area of this equatorial event, along with a recently installed continuous GPS array, made this among the best-observed megathrust events ever (Briggs et al. 2006). These data (Figure 12), along with survey-mode GPS and global seismic data, have been modeled extensively by several groups (e.g., Briggs et al. 2006, Hsu et al. 2006, Kreemer et al. 2006, Walker et al. 2005, Konca et al. 2006) to explain coseismic and postseismic deformation (Figure 13) associated with this event.

On the island of Simeulue, corals and GPS recorded details of how the 2004 and 2005 events' deformation fields overlapped, and they showed that an earlier event in 2002 split these deformation fields. When these records are taken together, the study illuminates an extraordinarily well-documented case of fault segmentation and a well-defined fault segment boundary. Because the forearc islands here overlie the seis-

mogenic portion of these ruptures, details of slip can be obtained. In particular, better-than-usual resolution of the shallow updip slip edge is possible in this case, allowing a study of how near slip went to the trench. Although there is alongstrike variation, it appears that, for much of the length of this rupture, slip terminated at about 15 km downdip from the trench. This appears to confirm the theory on the limit of updip slip and shallow transition to stable sliding (e.g., Byrne et al. 1988; Marone et al. 1991; Scholz 1989, 2002).

The observation that evidently little slip occurred at depths shallower than 15 km along much of the Nias-Simeulue rupture seems consistent with this event's lack of an associated severe tsunami. The overall source dimensions, however, were also far smaller for this event than for the Sumatra-Andaman event. The tsunami for this event, measured as 4 m in Banyak and 2–3 m in several places in Nias, may be considered small for one associated with an M=8.6 earthquake. This may also be, as explained by Briggs et al. (2006), the result of much of the ground deformation occurring along islands and in shallow water, so that the water column displacement and seafloor-to-water coupling was less than usual.

Interestingly, uplift in the 2004 and 2005 events was characterized by a topographic belt of uplift, or "saddle," and other features across Simeulue and Nias islands that appear to mimic the long-term deformation pattern, suggesting that a succession of similar earthquakes may have produced the islands' topography and adjoining straits' bathymetry over many years (Briggs et al. 2006). Evidently, the 1861 earthquake that was studied by Newcomb and McCann (1987) ruptured approximately the same segment of the Sunda megathrust that again ruptured in the 2005 Nias-Simeulue event. Furthermore, the low-slip (and presumably lower-friction) portions of the megathrust even appear to correspond to where the wedge taper is more gradual, in agreement with theory (e.g., Davis et al. 1983).

DISCUSSION

As the Sumatra-Andaman and Nias-Simeulue events have shown, earthquakes are in some ways extremely unpredictable. For example, because of the very oblique subduction from 5° N to 15° N, seismic and tsunami hazards had been considered zero or barely finite along what became the source of one of history's deadliest natural calamities. On the other hand, one of the major uncertainties in seismic hazard models involves rupture segmentation, and the data from these earthquakes have certainly proved illuminating in this regard. While some researchers discover new hope and optimism among these new findings, others point out that we are clearly still far from a comprehensive understanding. Are these natural phenomena inherently chaotic? Are the glimmers of predictability we observe within the system, such as the 2005 event's similarity to the 1861 event, or the evidently stationary nature of the Simeulue segment boundary, merely coincidental? For example, even if we were to obtain a perfect understanding of fault segmentation on Simeulue Island, we also must learn how ruptures may cascade from one segment to another.

The pause between stages in a rupture cascade may be rapid on the broad scale of geological time, but to humans a pause of anything between days and decades may seem lengthy. At least, such pauses give us a chance to model and try to anticipate what may come next (e.g., McCloskey et al. 2005, Sieh 2005, Pollitz et al. 2006b). A natural distinction in the time scale occurs, of course, for dynamic and static cases. Once the propagating waves have dissipated from the system, the static stress changes and any transient physical processes remain in effect and can continue forcing the cascading phenomenon. We ask such questions as "What is coseismic versus postseismic rupture?" or "Is this a cascading complex source with many subevents, or is it several discrete events?" The answers lie in recognizing the continuum in natural rupture phenomena. It is important to better define and consistently use terms meant to describe certain aspects of fault behavior such as "afterslip" or "slow slip."

While all of this may help in understanding earthquake source physics, it also means that sources are even more varied and complicated than we had realized before the advent of modern broadband seismic and continuous GPS data. That is, state-of-the-art global and regional data for these megathrust events have shown us details of the source that we could not have obtained for, say, either the 1960 Chile or 1964 Alaska event. Now we are able to pursue more pointed questions about source physics, taking advantage of all the new data. Our ability to model the source and propagation, as well as resultant deformation field, has certainly improved greatly in the last several decades. It is nevertheless clear that we would have benefited greatly from having more of certain types of data for these earthquakes. For example, for the Sumatra-Andaman event, continuous GPS data from the A&N Islands, as well as more water level data from the Indian Ocean, would allow us to better model the second half or northern portion of the earthquake source and how it related to the formation of the tsunami. We would do well to collectively instrument source areas of potential future megathrust events so as to capture, in even better detail, their source properties the next time we have such an opportunity to learn from nature.

If rupture propagates updip to the seafloor at the trench, producing large ground motions associated with primary faulting at the seafloor, and upward fling of the hanging wall, a large amount of energy is expected go into tsunamigenesis (Geist and Dmowska 1999). In contrast, blind rupture that is embedded and does not reach the trench is less likely to couple energy efficiently into the water column. Further modeling and analysis are needed to understand better the relationship between shallow faulting and tsunamigenesis. In some model studies, there is little difference between a "blind" rupture and one that does reach the seafloor. It seems possible that, despite the large amount of slip, both of these megathrust ruptures may have been "blind" (that is, the fault surface may not have broken up to the seafloor) although this is far from being well determined at this time. We lack firm direct evidence, for either the Sumatra-Andaman or the Nias-Simeulue events, of seafloor displacement at the trench itself. Whether rupture propagates to the seafloor or remains "blind" is thought to have very important implications for tsunamigenesis (e.g., Geist and Dmowska 1999, Geist 1999, Geist et al. 2006). Furthermore, no large-scale submarine slumps have yet been identified, despite attempts to document these potential contributors to the magnitude of the tsunami.

Of fundamental importance for earthquake source physics is our ability to image the source in detail. Recent studies have converged upon a stable range of slip models for the Sumatra-Andaman earthquake in particular (e.g., Chlieh et al. 2006, Banerjee et al. 2006). Earlier studies suffered from too few data, or overemphasis on one type of data (e.g., global teleseismic waveforms) that were effectively band-limited for an event of this size. A key lesson from this earthquake is that very-long-period data from geodesy (e.g., GPS vectors and time series) and geology (e.g., the uplift and subsidence of coral reefs) can be very important for the accurate definition of finite fault source properties such as overall length, width, and of course, slip distribution and rise time for slowly occurring slip. Modern earthquake monitoring now clearly needs to include continuous GPS observation, preferably at rates higher than or equal to one sample per second, rather than the usual 30- or 15-second sample interval. High-resolution earth-observing satellites are also crucial for defining the effects of earthquakes, as can be bathymetric swath mapping and deep submersibles for detailed studies of seafloor deformation associated with megathrust events.

ACKNOWLEDGMENTS

This paper is dedicated to the victims of these events. I am grateful to Bill Iwan, Hiroo Kanamori, and John Galetzka for the motivation and encouragement they provided. I thank my many colleagues who openly and generously shared initial results and preprints of their latest work ever since the event, especially Chen Ji and Mohamed Chlieh. Many of my colleagues' figures, along with associated captions, are reprinted here with their gracious permission. Importantly, the open sharing of data facilitated rapid production and dissemination of results after these earthquakes, to the benefit of all. The vast cumulative research effort by many institutions worldwide that is described within this overview has been supported by funding sources far too numerous to list individually, yet all are greatly appreciated collectively by the earthquake research community. I am also especially grateful for critical, incisive, and substantive reviews of the initial version of this paper provided by Hiroo Kanamori, Kerry Sieh, Jean-Philippe Avouac, Mohamed Chlieh, Rich Briggs, and Aron Meltzner (all at Caltech); and by Walter Mooney, Lucy Jones, Eric Geist, and Fred Pollitz (all at USGS).

REFERENCES

Aagaard, B. T., Hall, J. F., and Heaton, T. H., 2004. Effects of fault dip and slip rake angles on near-source ground motions: Why rupture directivity was minimal in the 1999 Chi-Chi, Taiwan, earthquake, *Bull. Seismol. Soc. Am.* **94**, 155–170.

Ammon, C. J., Ji, C., Thio, H. K., Robinson, D., Ni, S. D., Hjorleifsdottir, V., Kanamori, H., Lay, T., Das, S., Helmberger, D., Ichinose, G., Polet, J., and Wald, D., 2005. Rupture process of the 2004 Sumatra-Andaman earthquake, *Science* **308**, 1133–1139.

Banerjee, P., Pollitz, F., and Burgmann, R., 2005. Size and duration of the great 2004 Sumatra-Andaman earthquake from far-field static offsets, *Science* **308**, 1769–1772.

Banerjee, P., Pollitz, F., Nagarajan, B., and Burgmann, R., 2006. Coseismic slip distributions of the 26 December 2004 Sumatra-Andaman and 28 March 2005 Nias earthquakes from GPS static offsets, *Bull. Seismol. Soc. Am.*, in press.

Bettinelli, P., Avouac, J.-P., Flouzat, M., Jouanne, F., Bollinger, L., Willis, P., and Chitraker, G. R., 2006. Plate motion of India and interseismic strain in the Nepal Himalaya from GPS and DORIS measurements, *J. Geodesy*, doi: 10.1007//s00190–006–0030–3.

Bilham, R., 2005. A flying start, then a slow slip, *Science* **308**, 1126–1127.

Bilham, R., 2006. Personal communication.

Bilham, R., Engdahl, R., Feldl, N., and Satyabala, S. P., 2005. Partial and complete rupture of the Indo-Andaman plate boundary 1847–2004, *Seismol. Res. Lett.* **76**, 299–311.

Bird, P., and Kagan, Y. Y., 2004. Plate-tectonic analysis of shallow seismicity: Apparent boundary width, beta, corner magnitude, coupled lithosphere thickness, and coupling in seven tectonic settings, *Bull. Seismol. Soc. Am.* **94** (6), 2380–2399.

Briggs, R. W., Sieh, K., Meltzner, A. J., Natawidjaja, D., Galetzka, J., Suwargadi, B., Hsu, Y., Simons, M., Hananto, N., Suprihanto, I., Prayudi, D., Avouac, J.-P., Prawirodirdjo, L., and Bock, Y., 2006. Deformation and slip along the Sunda megathrust in the great 2005 Nias-Simeulue earthquake, *Science* **311**, 1897–1901.

Byrne, D. E., Davis, D., and Sykes, L., 1988. Loci and maximum size of thrust earthquakes and the mechanics of the shallow region of subduction zones, *Tectonics* **7**, 833–857.

Chlieh, M., Avouac, J.-P., Hjorleifsdottir, V., Song, T.-R. A., Ji, C., Sieh, K., Sladen, A., Hebert, H., Prawirodirdjo, L., Bock, Y., and Galetzka, J., 2006. Coseismic slip and afterslip of the Great (M_w 9.15) Sumatra-Andaman earthquake of 2004, *Bull. Seismol. Soc. Am.*, in press.

Curray, J. R., 2005. Tectonics and history of the Andaman Sea region, *J. Asian Earth Sciences* **25**, 187–232.

Davis, D., Suppe, J., and Dahlen, F. A., 1983. Mechanics of fold-and-thrust belts and accretionary wedges: Cohesive Coulomb theory, *J. Geophys. Res.* **88**, 1153–1172.

DeMets, C., Gordon, R., and Royer, J.-Y., 2005. Motion between the Indian, Capricorn, and Somalian plates since 20 Ma: Implications for the timing and magnitude of distributed lithospheric deformation in the equatorial Indian Ocean, *Geophys. J. Int.* **161**, 445–468.

Gahalaut, V. K., Nagarajan, B., Catherine, J. K., Subhash, K., and Sinha, M. S., 2006. Constraints on 2004 Sumatra-Andaman earthquake rupture from GPS measurements in Andaman-Nicobar Islands, *Earth Planet. Sci. Lett.* **242**, 365–374.

Geist, E. L., 1999. Local tsunamis and earthquake source parameters, in Dmowska, R. and Saltzman, B., (eds.), *Tsunamigenic Earthquakes and Their Consequences*, *Adv. Geophys.* **39**, 117–209.

Geist, E. L., and Dmowska, R., 1999. Local tsunamis and distributed slip at the source, *Pure Appl. Geophys.* **154**, 485–512.

Geist, E. L., Bilek, S. L., Arcas, D., and Titov, V. V., 2006. Differences in tsunami generation between the December 26, 2004 and March 28, 2005 Sumatra earthquakes, *Earth, Planets Space* **58**, 195–201.

Genrich, J. F., Bock, Y., McCaffrey, R., Prawirodirdjo, L., Stevens, C. W., Puntodewo, S. S. O., Subarya, C., and Wdowinski, S., 2000. Distribution of slip at the northern Sumatra fault system, *J. Geophys. Res.* **105** (28), 327–28, 341.

Giardini, D., Grünthal, G., Shedlock, K. M., and Zhang, P., 1999. The GSHAP Global Seismic Hazard Map, *Annali di Geofisica* **42**, 1225–1230.

Giardini, D., Grünthal, G., Shedlock, K., and Zhang, P., 2003. The GSHAP Global Seismic Hazard Map, in Lee, W., Kanamori, H., and Jennings, P. (eds.), *International Handbook of Earthquake and Engineering Seismology*, IASPEI, Elsevier Science and Technology, Oxford, UK.

Guilbert, J., Vergoz, J., Schissele, E., Roueff, A., and Cansi, Y., 2005. Use of hydroacoustic and seismic arrays to observe rupture propagation and source extent of the M_w=9.0 Sumatra earthquake, *Geophys. Res. Lett.* **32**, L15310, doi: 10.1029/2005GL022966.

Haines, A. J., and Holt, W. E., 1993. A procedure for obtaining the complete horizontal motions within zones of distributed deformation from the inversion of strain rate data, *J. Geophys. Res.* **98**, 12057–12082.

Hashimoto, M., Chhoosakul, N., Hashizume, M. S., Takemoto, S., Takiguchi, H., Fukada, Y., and Fujimori, K., 2006. Crustal deformations associated with the Great Sumatra-Andaman earthquake deduced from continuous GPS observation, *Earth, Planets Space* **58**, 127–139.

Heki, K., Miyazaki, S., and Tsuji, H., 1997. Silent fault slip following an interplate thrust earthquake at the Japan Trench, *Nature* **386**, 595–597.

Henstock, T. J., McNeill, L. C., and Tappin, D. R., 2006. Seafloor morphology of the Sumatran subduction zone: Surface rupture during megathrust earthquakes? *Geology*, in press.

Hirata, K., Satake, K., Tanioka, Y., Kuragano, T., Hasegawa, Y., Hayashi, Y., and Hamada, N., 2006. The 2004 Indian Ocean tsunami: Tsunami source model from satellite altimetry, *Earth, Planets Space* **58**, 195–201.

Hsu, Y.-J., Simons, M., Avouac, J.-P., Sieh, K., Galetzka, J., Chlieh, M., Bock, Y., Natawidjaja, D. H., and Prawirodirdjo, L., 2006. Frictional afterslip following the M_w 8.7, 2005 Nias earthquake, Sumatra, *Science* (submitted).

Jade, J., Ananda, M. B., Dileep Kumar, P., and Banerjee, S., 2005. Co-seismic and post-seismic displacements in Andaman and Nicobar Islands from GPS measurements, *Curr. Sci.* **88**, 1980–1984.

Ji, C., Helmberger, D. V., Wald, D. J., and Ma, K. F., 2003. Slip history and dynamic implications of the 1999 Chi-Chi, Taiwan, earthquake, *J. Geophys. Res.* **108** (B9), 2412.

Kanamori, H., 1978. Quantification of earthquakes, *Nature* **271**, 411–414.

Kanamori, H., 2006. Seismological aspects of the December 2004 Sumatra-Andaman earthquake, *2004 Great Sumatra Earthquakes and Indian Ocean Tsunamis of December 26, 2004 and March 28, 2005*, *Earthquake Spectra* **22** (S4), June (this issue).

Konca, A. O., Hjorleifsdottir, V., Song, T.-R. A., Avouac, J.-P., Helmberger, D., Ji, C., Sieh, K., Briggs, R., and Meltzner, A., 2006. Rupture kinematics of the 2005 M_w 8.6 Nias-Simeulue earthquake from the joint inversion of seismic and geodetic data, *Bull. Seismol. Soc. Am.*, in press.

Kreemer, C., Haines, A. J., Holt, W. E., Blewitt, G., and Lavallée, D., 2000a. On the determination of a global strain rate model, *Earth, Planets Space* **52**, 765–770.

Kreemer, C., Holt, W. E., Goes, S., and Govers, R., 2000b. Active deformation in eastern Indonesia and the Philippines from GPS and seismicity data, *J. Geophys. Res.* **105**, 663–680.

Kreemer, C., Holt, W. E., and Haines, A. J., 2003. An integrated global model of present-day plate motions and plate boundary deformation, *Geophys. J. Int.* **154** (1), 8–34.

Kreemer, C., Blewitt, G., Hammond, W. C., and Plag, H. P., 2006. Global deformation from the Great 2004 Sumatra-Andaman earthquake observed by GPS: Implications for rupture process and global reference frame, *Earth, Planets Space* **58**, 141–148.

Lay, T., Kanamori, H., Ammon, C. J., Nettles, M., Ward, S. N., Aster, R. C., Beck, S. L., Bilek, S. L., Brudzinski, M. R., Butler, R., DeShon, H. R., Ekstrom, G., Satake, K., and Sipkin, S., 2005. The great Sumatra-Andaman earthquake of 26 December 2004, *Science* **308**, 1127–1133.

Marone, C., Scholz, C., and Bilham, R., 1991. On the mechanics of earthquake afterslip, *J. Geophys. Res.* **96**, 8441–8452.

McCaffrey, R., Zwick, P., Bock, Y., Prawirodirdjo, L., Genrich, J., Stevens, C. W., Puntodewo, S. S. O., and Subarya, C., 2000. Strain partitioning during oblique plate convergence in northern Sumatra: Geodetic and seismologic constraints and numerical modeling, *J. Geophys. Res.* **105**, 28,363–28,376.

McCann, W. R., Nishenko, S. P., Sykes, L. R., and Krause, J., 1979. Seismic gaps and plate tectonics: Seismic potential for major boundaries, *Pure Appl. Geophys.* **117**, 1082–1147.

McCloskey, J., Nalbant, S. S., and Steacy, S., 2005. Earthquake risk from co-seismic stress, *Nature* **434**, 291.

Melbourne, T., Carmichael, I., DeMets, C., Hudnut, K. W., Sanchez, O., Stock, J., Suarez, G., and Webb, F., 1997. The geodetic signature of the M8.0 October 9, 1995 Jalisco subduction earthquake, *Geophys. Res. Lett.* **24** (6), 715–718.

Melbourne, T. I., Webb, F. H., Stock, J. M., and Reigber, C., 2002. Rapid postseismic transients in subduction zones from continuous GPS, *J. Geophys. Res., [Solid Earth]* **107**, 2241.

Meltzner, A. J., 2006. Personal communication.

Meltzner, A. J., Sieh, K., Abrams, M., Agnew, D. C., Hudnut, K. W., Avouac, J.-P., and Natawidjaja, D. H., 2006. Uplift and subsidence associated with the great Aceh-Andaman earthquake of 2004, *J. Geophys. Res.* **111**, B02407, doi: 10.1029/2005JB003891.

Moran, K., and Tappin, D., 2006. *SEATOS 2005 Cruise Report: Sumatra Earthquake and Tsunami Offshore Survey* (*SEATOS*). Available at http://ocean.oce.uri.edu/seatos/

Nalbant, S. S., Steacy, S., Sieh, K., Natawidjaja, D., and McCloskey, J., 2005. Earthquake risk on the Sunda Trench, *Nature* **435**, 756–757.

Nambath, S., 2005. A battered archipelago, *Frontline* **22** (2), 15–18 January. http://www.flonnet.com/fl2202/stories/20050128003402300.htm

Natawidjaja, D., Sieh, K., Ward, S., Cheng, H., Edwards, R. L., Galetzka, J., and Suwargadi, B., 2004. Paleogeodetic records of seismic and aseismic subduction from central Sumatran microatolls, Indonesia, *J. Geophys. Res.* **109**, doi: 10.1029/2003JB0002398.

Natawidjaja, D., Sieh, K., Chlieh, M., Galetzka, J., Suwargadi, B., Cheng, H., Edwards, R. L., Avouac, J.-P., and Ward, S., 2006. The giant Sumatran megathrust ruptures of 1797 and 1833: Paleoseismic evidence from coral microatolls, *J. Geophys. Res.*, in review.

Neetu, S., Suresh, I., Shankar, R., Shankar, D., Shenoi, S. S. C., Shetye, S. R., Sundar, D., and Nagarajan, B., 2005. Comment on "The Great Sumatra-Andaman Earthquake of 26 December 2004," *Science* **310**, 1431.

Newcomb, K., and McCann, W., 1987. Seismic history and seismotectonics of the Sunda arc, *J. Geophys. Res.* **92**, 421–439.

Pacheco, J. F., and Sykes, L. R., 1992. Seismic moment catalog of large shallow earthquakes, 1900 to 1989, *Bull. Seismol. Soc. Am.* **82**, 1306–1349.

Paul, J., Burgmann, R., Gaur, V. K., Bilham, R., Larson, K. M., Ananda, M. B., Jade, S., Mukal, M., Anupama, T. S., Satyal, G., and Kumar, D., 2001. The motion and active deformation of India, *Geophys. Res. Lett.* **28**, 647–650.

Perfettini, H., and Avouac, J.-P., 2004. Postseismic relaxation driven by brittle creep: A possible mechanism to reconcile geodetic measurements and the decay rate of aftershocks, application to the Chi-Chi earthquake, Taiwan, *J. Geophys. Res.* **109**, B02304, doi: 10129/2003JB002488.

Petersen, M. D., Mueller, C., Harmsen, S., Frankel, A. D., Rukstales, K., Dewey, J., and Hartzell, S., 2004. Probabilistic seismic hazard analysis for Sumatra, Indonesia and across the southern Malaysian Peninsula, *Tectonophysics* **390**, 141–158.

Pollitz, F. F., Banerjee, P., and Burgmann, R., 2006a. Postseismic relaxation following the great 2004 Sumatra-Andaman earthquake on a compressible self-gravitating Earth, *Geophys. J. Int.*, accepted.

Pollitz, F. F., Banerjee, P., Burgmann, R., Hashimoto, M., and Chooksakul, N., 2006b. Stress changes along the Sunda trench following the 26 December 2004 Sumatra-Andaman and 28 March Nias earthquakes, *Geophys. Res. Lett.* **33**, L06309, doi: 10.1029/2005GL024558.

Prawirodirdjo, L., Bock, Y., McCaffrey, R., Genrich, J., Calais, E., Stevens, C., Puntodewo, S. S. O., Subarya, C., and Rais, J., 1997. Geodetic observations of interseismic strain segmentation at the Sumatra subduction zone, *Geophys. Res. Lett.* **24**, 2601–2604.

Scholz, C., 1989. Mechanics of faulting, *Annu. Rev. Earth Planet Sci.* **17**, 309–334.

Scholz, C. H., 2002. *The Mechanics of Earthquakes and Faulting*, 2nd edition, Cambridge University Press, Cambridge, UK, 496 pp.

Sella, G. F., Dixon, T. H., and Mao, A., 2002. REVEL: A model for recent plate velocities from space geodesy, *J. Geophys. Res.* **107**, 2081.

Shedlock, K. M., Giardini, D., Grünthal, G., and Zhang, P., 2000. The GSHAP Global Seismic Hazard Map, *Seismol. Res. Lett.* **71** (6), 679–686.

Sieh, K., 2005. Aceh-Andaman earthquake: What happened and what's next? *Nature* **434**, 573–574.

Socquet, A., Vigny, C., Chamot-Rooke, N., Simons, W., Rangin, C., and Ambrosius, B., 2006. India and Sunda Plates motion and deformation along their boundary in Myanmar determined by GPS, *J. Geophys. Res.*, submitted.

Subarya, C., Chlieh, M., Prawirodirdjo, L., Avouac, J.-P., Bock, Y., Sieh, K., Meltzner, A., Natawidjaja, D., and McCaffrey, R., 2006. Plate-boundary deformation associated with the great Sumatra-Andaman earthquake, *Nature* **440**, 46–51.

Tobita, M., Suito, H., Imakiire, T., Kato, M., Fujiwara, S., and Murakami, M., 2006. Outline of vertical displacement of the 2004 and 2005 Sumatra earthquakes revealed by satellite radar imagery, *Earth, Planets Space* **58**, e1–e4.

Vigny, C., Simons, W. J. F., Abu, S., Bamphenyu, R., Satirapod, C., Choosakul, N., Subarya, C., Socquet, A., Omar, K., Abidin, H. Z., and Ambrosius, B. A. C., 2005. Insight into the 2004 Sumatra-Andaman earthquake from GPS measurements in southeast Asia, *Nature* **436**, 201–206.

Walker, K. T., Ishii, M., and Shearer, P. M., 2005. Rupture details of the 28 March 2005 Sumatra M_w 8.6 earthquake imaged with teleseismic *P* waves, *Geophys. Res. Lett.* **32**, L24303, doi: 10.1029/2005GL024395.

Zachariasen, J., Sieh, K., Taylor, F. W., Edwards, R. L., and Hantoro, W. S., 1999. Submergence and uplift associated with the giant 1833 Sumatran subduction earthquake: Evidence from coral microatolls, *J. Geophys. Res.* **104** (B1), 895–920.

(Received 20 March 2006; accepted 24 May 2006)